A new method for the simultaneous measurement of magnitude and sign of $^1\text{D}_{\text{CH}}$ and $^1\text{D}_{\text{HH}}$ dipolar couplings in methylene groups*

Teresa Carlomagno[a,**], Wolfgang Peti[a] & Christian Griesinger[a,b,***]
[a]*Institut für Organische Chemie, Universität Frankfurt, Marie-Curie Strasse 11, D-60439 Frankfurt, Germany;*
[b]*Max-Planck Institute for Biophysical Chemistry, Am Faßberg 11, D-37077 Göttingen, Germany*

Abstract

Heteronuclear dipolar couplings of the protein backbone have proven to have a big impact on the accuracy of protein NMR structures. H,H dipolar couplings might have the same impact on side chains. Here we present a method that combines both heteronuclear and homonuclear dipolar couplings to investigate the local conformation of methylene groups. A new pulse sequence (SPITZE-HSQC) is presented, that allows to measure the two C,H and the H,H dipolar couplings at the same time, using spin state selective transfers. The new method has been applied to the methylene groups of glycines in the protein ubiquitin. The C,H and the H,H dipolar couplings might have a key role in fast stereospecific assignment of protons in CH_2 groups.

Abbreviations: S_3E, spin state selection; HSQC, heteronuclear single quantum correlation; TOCSY, total correlated spectroscopy.

Introduction

Dipolar couplings (Tolman et al., 1995; Tjandra and Bax, 1997) constitute a powerful tool to obtain long-range structural restraints. Residual heteronuclear dipolar couplings have a special impact on structural studies of multidomain proteins (Fischer et al., 1999) where long range restraints are needed to define the orientation of one domain with respect to the other. The size and the sign of residual dipolar couplings can be measured from the difference of the splitting observed in partially aligned and isotropic solutions of the molecule, provided that the amount of alignment is so weak that the absolute value of the dipolar coupling is smaller than the absolute value of the scalar coupling. Dipolar couplings can be used to obtain

local information as well. Here we introduce a new method to measure D_{CH_1}, D_{CH_2} and $D_{H_1H_2}$ dipolar couplings in methylene groups through an S^3E-type HSQC (Meissner et al., 1997) in aligned solutions. The sign of the $D_{H_1H_2}$ coupling is obtained as well.

Local structural information on methylene groups is particularly important for hydrophobic side chains located in protein cores. The D_{CH} and D_{HH} couplings can be used to refine the local environment and to obtain the stereospecific assignment of the protons, provided that additional structural information is known. Recently, a method for the measurement of methylene and methyl dipolar couplings has been reported (Ottiger et al., 1998). In this work only the sum of the two CH dipolar couplings in methylene groups could be measured and several spectra needed to be recorded to obtain an accurate fit of the experimental data. With the present approach dipolar couplings for each individual CH vector and also for the HH vector can be easily measured from only four experiments. The H,H dipolar coupling provides additional infor-

A

$H_1^-H_2^\beta C^\alpha$ $H_1^-H_2^\alpha C^\alpha$ $H_1^-H_2^\beta C^\beta$ $H_1^-H_2^\alpha C^\beta$

5 6   7 8

$C^-H_1^\beta H_2^\beta$

$C^-H_1^\alpha H_2^\beta$
$C^-H_1^\beta H_2^\alpha$

$C^-H_1^\alpha H_2^\alpha$

1 2   3 4

$^1J_{CH_1} + {}^1J_{CH_2}$

$\omega_1(^{13}C)$

$^1J_{CH_1}$

$\omega_2(^1H)$

$^2J_{H_1H_2}$

B

S_1 0   −1   1   0

$H_1^- H_2^\beta C^\alpha$ $H_1^- H_2^\alpha C^\alpha$ $H_1^- H_2^\beta C^\beta$ $H_1^- H_2^\alpha C^\beta$

7

1 $C^-H_1^\beta H_2^\beta$

0 $C^-H_1^\beta H_2^\alpha$
0 $C^-H_1^\alpha H_2^\beta$

$^1J_{CH_2} + {}^1D_{CH_2}$

$^1J_{CH_1} + {}^1D_{CH_1}$

−1 $C^-H_1^\alpha H_2^\alpha$

2

C^-

H_1^-

$^2J_{H_1H_2} + D_{H_1H_2}$

C

$H_1^- H_2^\beta C^\alpha$ $H_1^- H_2^\alpha C^\alpha$ $H_1^- H_2^\beta C^\beta$ $H_1^- H_2^\alpha C^\beta$

8

$^1J_{CH_2} + {}^1D_{CH_2}$

$^1J_{CH_1} + {}^1D_{CH_1}$

1
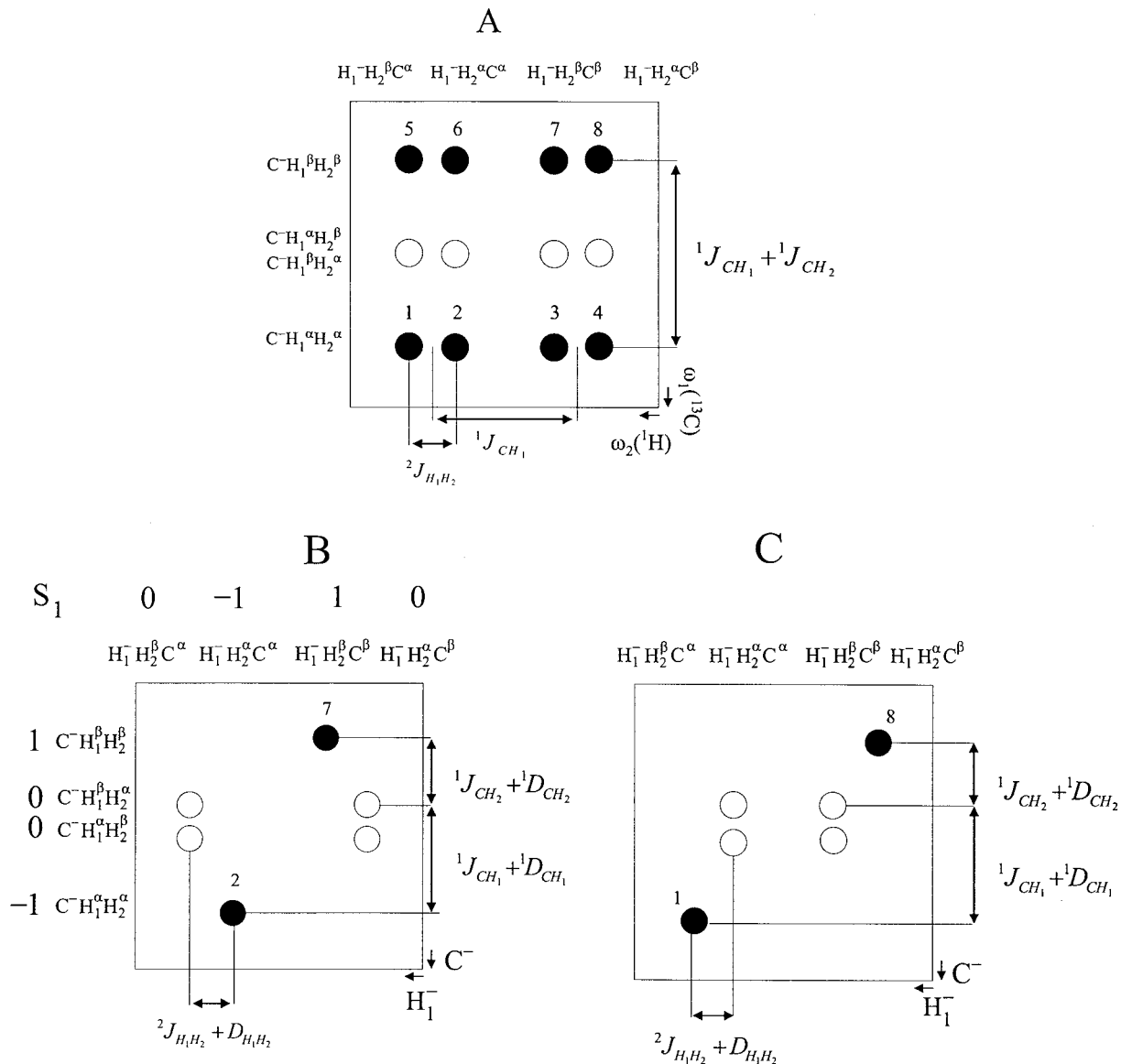
C^-

H_1^-

$^2J_{H_1H_2} + D_{H_1H_2}$

Figure 1. (A) Schematic representation of the peak deriving from a CH_1H_2 group at the frequency of the carbon in ω_1 and of proton H_1 in ω_2. The central lines (empty circles) are missing provided that J_{CH_1} and J_{CH_2} are equal. The splitting in ω_1 equals the sum of the two coupling constants $J_{CH_1} + J_{CH_2}$. Peaks 1 and 2, 3 and 4, 5 and 6, and 7 and 8 are separated by the $J_{H_1H_2}$ couplings, and they are generally not resolved in proteins due to the large linewidth. (B and C) Schematic representation of the selection rules for the mixing operators $\mathbf{H}_1 = \pi(J_{CH_1} + D_{CH_1})(C_x H_{1x} + C_y H_{1y}) + \pi(J_{CH_2} + D_{CH_2})(C_x H_{2x} + C_y H_{2y})$ in case $J_{CH_1} + D_{CH_1} \neq J_{CH_2} + D_{CH_2}$. The selection rules were derived classifying the coherences according to the symmetry operators $S_1 = C_z H_{1z} + C_z H_{2z}$ and $S_2 = H_{1z} + H_{2z} + C_z$, which commutes with both $\mathbf{H}_1$ and with the free evolution Hamiltonian. The eigenvalues of all coherences ρ for S_2 are: $[S_2, \rho] = -\rho$. Panel B gives the transfer pattern for the sequence of Figure 3 and panel C for the sequence of Figure 4.

mation with respect to the two C,H dipolar couplings, as shown in simulations, and the combination of the three dipolar couplings restricts the methylene group to four symmetry related orientations.

Theory

A schematic representation of a fully coupled HSQC (Müller, 1979; Bodenhausen and Ruben, 1980) for a CH_1H_2 group at the frequency of the carbon in ω_1 and of proton H_1 in ω_2 is reported in Figure 1A. The central lines (empty circles) are missing since the two contributions from $C^-H_1^\alpha H_2^\beta$ and $C^-H_1^\beta H_2^\alpha$ cancel out, provided that $J_{CH_1} + D_{CH_1}$ and $J_{CH_2} + D_{CH_2}$ are equal. The splitting in ω_1 equals the sum of the two coupling constants $J_{CH_1} + D_{CH_1} + J_{CH_2} + D_{CH_2}$. The peaks that appear in a coupled HSQC are the dark gray ones, which have been numbered in the figure from 1 to 8. Peaks 1 and 2, 3 and 4, 5 and 6, and 7 and 8 are separated by the $J_{H_1H_2} + D_{H_1H_2}$ couplings, and they are generally not resolved in proteins due to the large linewidth. The experiment we are going to describe achieves selective transfer between the following operators through a S^3E scheme:

$$C^-H_1^\alpha H_2^\alpha \rightarrow H_1^- H_2^\beta C^\alpha \qquad \text{peak 1} \qquad (1)$$
$$C^-H_1^\beta H_2^\beta \rightarrow H_1^- H_2^\alpha C^\beta \qquad \text{peak 8}$$

or

$$C^-H_1^\alpha H_2^\alpha \rightarrow H_1^- H_2^\alpha C^\alpha \qquad \text{peak 2} \qquad (2)$$
$$C^-H_1^\beta H_2^\beta \rightarrow H_1^- H_2^\beta C^\beta \qquad \text{peak 7}$$

This provides high reduction of spectral overlap and the possibility to measure all three involved couplings. Four spectra are obtained, each of which contains only one peak per CH$_2$ group. For partially aligned systems, the selectivity is independent of the identity of the couplings $J_{CH_1} + D_{CH_1}$ and $J_{CH_2} + D_{CH_2}$. The selective transfer presented here has several advantages in comparison to a coupled HSQC. First, for large molecules, where peaks 1 (8) and 2 (7) are in general not at all or only partially resolved, this approach allows the measurement of $J_{H_1H_2} + D_{H_1H_2}$ coupling constants, as peaks 1 (8) and 2 (7) now appear in two different spectra. Second, whereas the $J_{CH_1} + D_{CH_1}$ and $J_{CH_2} + D_{CH_2}$ couplings are measurable also in a coupled HSQC, the new approach allows the separation of the corresponding lines in two spectra, with greatly reduced spectral overlap. Third, due to the selectivity of the transfer described in Equations 1 and

2, the magnetization corresponding to the $C^-H_1^\alpha H_2^\alpha$ and the $C^-H_1^\beta H_2^\beta$ terms is not distributed on four lines, as in a coupled HSQC, but concentrated on one single line with maximum possible transfer efficiency (Glaser et al., 1998). This leads to a gain of a factor 4 in signal-to-noise with respect to a coupled HSQC for molecules for which the $J_{H_1H_2}$ coupling is resolved, and of a factor 2 for those molecules for which the $J_{H_1H_2} + D_{H_1H_2}$ coupling is not resolved, as has been found in spectra of diacetonglucose (data not shown).

The design of the new pulse sequence, which we call SPITZE-HSQC (SPIn sTate selective ZEro overlap HSQC), can be understood most easily in terms of selection of desired transitions in an energy level diagram (Figure 2). We will describe the design of the pulse sequence which achieves the operator transfers of Equation 1. The following explanation is rigorously valid only assuming $J_{CH_1} + D_{CH_1} = J_{CH_2} + D_{CH_2}$. The energy level diagram is that of two protons which sum up to a spin 1 and a spin 0 particle coupled to ^{13}C, which is the spin 1/2. The spin 0 of the two protons is not excited assuming equal $J_{CH} + D_{CH}$ couplings and is thus ignored in the level diagram. The energy level diagram consists of the following six levels: $|\alpha, 1\rangle$, $|\alpha, 0\rangle$, $|\alpha, -1\rangle$, $|\beta, 1\rangle$, $|\beta, 0\rangle$ and $|\beta, -1\rangle$, where for example $|\alpha, 0\rangle$ means that the carbon is in the α spin state and the spin 1 particle formed by the two protons has $F_z = H_{1z} + H_{2z} = 0$. These levels can be expressed as product functions with $|\alpha_C/\beta_C\rangle$ referring to carbon in the α or β state:

$$
\begin{aligned}
|\alpha/\beta, 1\rangle &= |\alpha_C/\beta_C\rangle |\alpha_{H_1}\rangle |\alpha_{H_2}\rangle \\
|\alpha/\beta, 0\rangle &= \frac{1}{\sqrt{2}} |\alpha_C/\beta_C\rangle \left(|\alpha_{H_1}\rangle |\beta_{H_2}\rangle \right. \\
&\quad \left. + |\beta_{H_1}\rangle |\alpha_{H_2}\rangle \right) \qquad (3) \\
|\alpha/\beta, -1\rangle &= |\alpha_C/\beta_C\rangle |\beta_{H_1}\rangle |\beta_{H_2}\rangle
\end{aligned}
$$

The operators $C^-H_1^\alpha H_2^\alpha = |\beta, 1\rangle \langle \alpha, 1|$ and $C^-H_1^\beta H_2^\beta = |\beta, -1\rangle \langle \alpha, -1|$ describe the two transitions indicated respectively with continuous and dashed black arrows in Figure 2A. These operators must be transferred selectively to the terms $(H_1^- H_2^\alpha C^\alpha + H_2^- H_1^\alpha C^\alpha) = \sqrt{2} |\alpha, 0\rangle \langle \alpha, 1|$ and $(H_1^- H_2^\beta C^\beta + H_2^- H_1^\beta C^\beta) = \sqrt{2} |\beta, -1\rangle \langle \beta, 0|$, respectively, which correspond to the two transitions indicated with continuous and dashed black arrows in Figure 2B. These selective transfers are obtained interchanging the energy levels that are connected by the wavy lines in Figure 2A. Both transfers are brought about by a zero quantum rotation $C_x F_x + C_y F_y$ by an
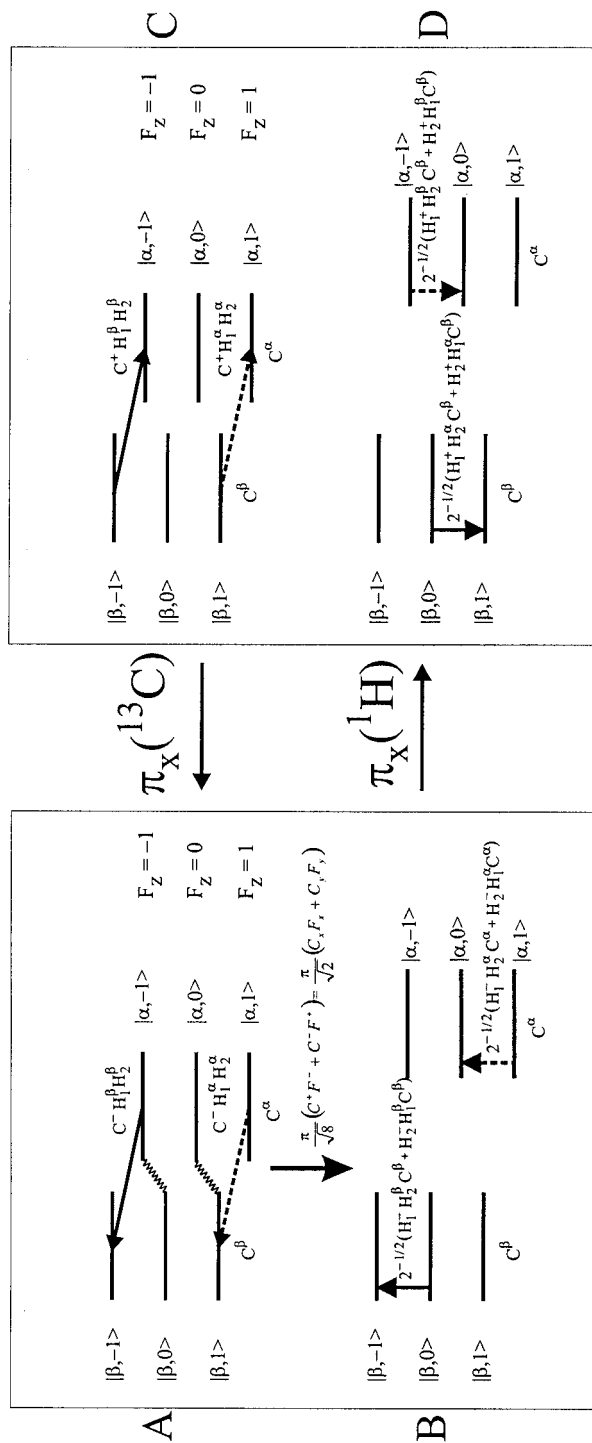
2 and 7

1 and 8

$\pi_x(^{13}C)$

$\pi_x(^1H)$

A

B

C

D

$F_z = -1$
$F_z = 0$
$F_z = 1$

$|\alpha,-1\rangle$
$|\alpha,0\rangle$
$|\alpha,1\rangle$

$|\beta,-1\rangle$
$|\beta,0\rangle$
$|\beta,1\rangle$

$C^-H_1^\beta H_2^\beta$
$C^-H_1^\alpha H_2^\alpha$
C^α
C^β

$\frac{\pi}{\sqrt{8}}(C^+F_- + C^-F_+) = \frac{\pi}{\sqrt{2}}(C_x F_x + C_y F_y)$

$2^{-1/2}(H_1^- H_2^\beta C^\beta + H_2^- H_1^\beta C^\beta)$

$2^{-1/2}(H_1^- H_2^\alpha C^\alpha + H_2^- H_1^\alpha C^\alpha)$

C^α
C^β

$C^+H_1^\beta H_2^\beta$
$C^+H_1^\alpha H_2^\alpha$
C^α
C^β

$2^{-1/2}(H_1^+ H_2^\alpha C^\beta + H_2^+ H_1^\alpha C^\beta)$

$2^{-1/2}(H_1^+ H_2^\beta C^\beta + H_2^+ H_1^\beta C^\beta)$

C^α
C^β

Figure 2. Symmetry adapted energy level diagram for a CH_1H_2 group. The arrows represent the desired transitions of Equations 1 and 2 in ω_1 (panel A) and ω_2 (panel B). The two levels connected by wavy lines must be interchanged to obtain the desired selective transfers, as explained in the text. For the selection of peaks 1 and 8, a $\pi_x(^{13}C)$ is introduced before the mixing, which transforms the coherences of C into A. Then the mixing from A to B is applied and finally the coherences are transformed to those in D by a $\pi_x(^1H)$ pulse. Altogether the transfer $C^+ \rightarrow H^+$ is shown. The desired transfer $C^- \rightarrow H^-$ is obtained with equal efficiency due to the hermiticity of all Hamiltonians in NMR.

angle $\pi/\sqrt{2}$:

$$e^{i\frac{\pi}{\sqrt{8}}(F^+C^-+F^-C^+)}|\beta,1\rangle\langle\alpha,1|e^{-i\frac{\pi}{\sqrt{8}}(F^+C^-+F^-C^+)} =$$

$$e^{i\frac{\pi}{2}(|\alpha,-1\rangle\langle\beta,0|+|\alpha,0\rangle\langle\beta,1|+|\beta,1\rangle\langle\alpha,0|+|\beta,0\rangle\langle\alpha,-1|)}$$

$$|\beta,1\rangle\langle\alpha,1| \tag{4}$$

$$e^{-i\frac{\pi}{2}(|\alpha,-1\rangle\langle\beta,0|+|\alpha,0\rangle\langle\beta,1|+|\beta,1\rangle\langle\alpha,0|+|\beta,0\rangle\langle\alpha,-1|)} =$$

$$i\,|\alpha,0\rangle\langle\alpha,1|$$

The rotation operator $(\pi/\sqrt{2})(C_xF_x + C_yF_y)$ is implemented in the following way: $\pi J(C_xF_x+C_zF_z))$ is implemented by a heteronuclear DIPSI (Shaka et al., 1988; Rucker and Shaka, 1989), leading to a rotation by $\pi/\sqrt{2}$ after $\tau = 1/\sqrt{2}(J_{CH} + D_{CH})$; application of $90^\circ_x(^1H,\ ^{13}C)$ and $90^\circ_{-x}(^1H,^{13}C)$ pulses before and after the DIPSI sequence, respectively transforms this Hamiltonian into the desired zero quantum rotation operator. The pulse sequence is shown in Figure 3A and delivers peaks 2 and 7 of Figure 1; the quadrature detection in t_1 is obtained by echo–antiecho selection. Evolution of homonuclear scalar couplings and dipolar couplings has no influence on the selectivity of the transfer since the functions of Equation 3 are eigenfunctions for the J-coupling Hamiltonian $2\pi J_{12}\vec{H}_1 \cdot \vec{H}_2$ and for the dipolar coupling Hamiltonian, which for the DIPSI mixing sequence in Figure 3A is $-\pi D_{12}(H_{1z}H_{2z} - \frac{1}{2}(H_{1x}H_{2x} + H_{1y}H_{2y}))$ on resonance.

Selection of peaks 1 and 8 is achieved by introduction of a $180^\circ_x(^{13}C)$ pulse before and $180^\circ_x(^1H)$ pulse after the zero quantum rotation, as indicated in Figures 2C and D. The transfer is depicted there for $C^+ \rightarrow H^+$. Due to the hermicity of all operators, the transfer $C^- \rightarrow H^-$ occurs with equal efficiency. The pulse sequence for this transfer (Figure 4A) is derived from the pulse sequence in Figure 3A by appending a $180^\circ_x(^{13}C)$ pulse before and a $180^\circ_x(^1H)$ pulse after the mixing performed in Figure 3A.

The peaks 2 and 7 as well as 1 and 8 of the schematic pulse sequence of Figures 3A and 4A, respectively, can be separated in two different spectra by an S^{3}E-type selection after the TOCSY transfer (Figures 3B,C and 4B,C). The two final spectra are obtained by adding and subtracting the two experiments of Figures 3 B and C and of Figures 4B and C, respectively. In the sequence of Figure 3B, the magnetization terms present at point a and corresponding to peaks 2 and 7 can be represented by the two arrows of Figure 5A. These terms defocus with respect to the $J_{CH} + D_{CH}$ couplings for a total delay $1/(4(J_{CH} + D_{CH}))$, during which they acquire a phase difference of 90° ($\pm 45^\circ$). In the experiment of Figure 3B, no
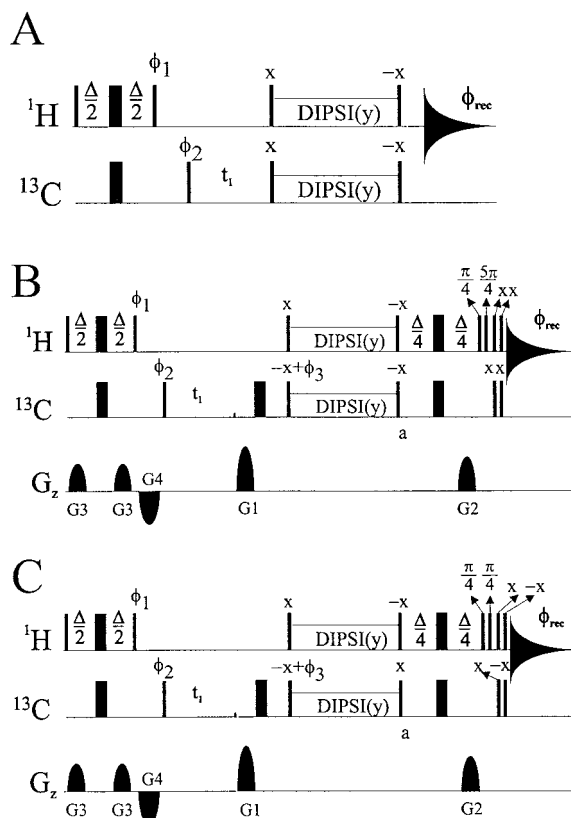

Figure 3. (A) Schematic sequence which implements the zero quantum Hamiltonian for the selection of peaks 2 and 7. The DIPSI sequence is along y and is irradiated with a field of 6250 Hz. (B and C) Pulse sequences for the selection of peaks 2 and 7 and their separation in two spectra. All pulses are hard. Phases not explicitly given are equal to x; $\phi_1 = $ y, $-$y; $\phi_2 = $ x, x, $-$x, $-$x; $\phi_{rec.} = $ x, $-$x, x, $-$x. Gradients are G1 = 4G2. Quadrature detection in t_1 is achieved by adding and subtracting two FIDS acquired with $\phi_3 = 0$, G1 = 4G2 and $\phi_3 = \pi$, G1 = $-$4G2 in the experiment of panels B and C. The experiments resulting from the pulse sequences of panels B and C must be added and subtracted to obtain the desired separation. The two $180^\circ_x(^{13}C,^1H)$ pulses before the acquisition time can be shifted after the TOCSY mixing and before the defocusing delay $\Delta/2$ and therefore translated into a phase shift of the 90° pulse flanking the TOCSY mixing on the corresponding nucleus. This achieves a reduction of the number of pulses needed for the desired selection.

effective pulse is applied at the end of this delay. The experiment of Figure 3C differs from the experiment of Figure 3B until point a by a $180^\circ_x(^{13}C)$ pulse; therefore peaks 4 and 5 are selected instead of peaks 2 and 7 from the TOCSY sequence. The two $180^\circ_x(^{13}C,^1H)$ pulses during the defocusing delay $1/(4(J_{CH} + D_{CH}))$ transform them in peaks 1 and 8. At the end of this delay a 180° pulse with 45° phase is applied to the proton. This pulse turns the magnetization corresponding to peaks 1 and 8 in 2 and 7 (with negative amplitude),

Table 1. $J_{H_1 H_2}$, J_{CH_1} and J_{CH_2} scalar couplings for glycines in non-oriented ubiquitin (columns 1–3); $D_{H_1 H_2}$, D_{CH_1} and D_{CH_2} experimental (columns 4–6) and calculated (columns 7–9 (X-RAY) and 10–12 (NMR)) dipolar couplings for glycines in oriented ubiquitin (details are given in the text). The error of measurement of the couplings is ±0.4 Hz.

	Non-oriented ubiquitin scalar couplings			Oriented ubiquitin: dipolar couplings			Theoretical dipolar couplings (X-RAY)			Theoretical dipolar couplings (NMR)		
	J_{H1H2} (Hz)	J_{CH1} (Hz)	J_{CH2} (Hz)	D_{H1H2} (Hz)	D_{CH1} (Hz)	D_{CH2} (Hz)	D_{H1H2} (Hz)	D_{CH1} (Hz)	D_{CH2} (Hz)	D_{H1H2} (Hz)	D_{CH1} (Hz)	D_{CH2} (Hz)
Gly10	−17.6	143.7	142.4	−12	52.3	−16.6	−19.9	43.4	−33.6	−14.1	64.5	−24.8
Gly35	−16.5	145.2	142.8	18.7			21.6	−33.9	94.2	36.1	−31.4	118.0
Gly47	−17.6	143.4	139.5	−34.2	45.5	−29.4	−12.8	58.6	−44.1	−25.8	53.3	−39.7
Gly75	−16.6	142.3	142.3	−3.0	8.3	8.3	4.9	32.7	−44.8	−25.0	0.0	−78.4
Gly76	−17.3	140.4	140.6	−1.9	4.8	4.4	−37.6	−39.5	−31.9	−19.5	−9.0	−62.8

A

^{1}H

^{13}C

B

^{1}H

^{13}C

G$_z$

C

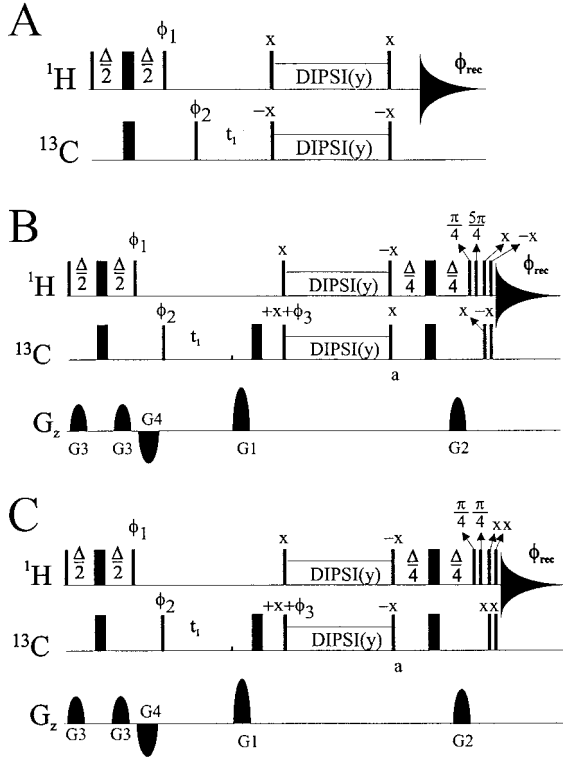^{1}H

^{13}C

G$_z$

Figure 4. (A) Schematic sequence for the selection of peaks 1 and 8, obtained adding a $180_x^\circ(^{13}$C) pulse before and a $180_x^\circ(^1$H) pulse after the mixing time of Figure 3A. The DIPSI sequence is along y and is irradiated with a field of 6250 Hz. (B and C) Pulse sequences for the selection of peaks 1 and 8 and their separation in two spectra. All pulses are hard. Phases not explicitly given are equal to x; $\phi_1 =$ y, $-$y; $\phi_2 =$ x, x, $-$x, $-$x; $\phi_{rec.} =$ x, $-$x, x, $-$x. Gradients are G1 = 4G2. Quadrature detection in t_1 is achieved by adding and subtracting two FIDS acquired with $\phi_3 = 0$, G1 = 4G2 and $\phi_3 = \pi$, G1 = $-$4G2 in the experiment of panels B and C. The experiments resulting from the pulse sequences of panels B and C must be added and subtracted to obtain the desired separation. The two $180_x^\circ(^{13}$C,^{1}H) pulses before the acquisition time can be shifted after the TOCSY mixing and before the defocusing delay $\Delta/2$ and therefore translated into a phase shift of the 90° pulse flanking the TOCSY mixing on the corresponding nucleus. This achieves a reduction of the number of pulses needed for the desired selection.

respectively. Adding and subtracting the two experiments 3B and 3C, separation of the peaks 2 and 7 in two different spectra is obtained. Analogously, the two sequences of Figures 4B,C achieve separation of the peaks 1 and 8 in two spectra. Since the $J_{CH} + D_{CH}$ couplings are different for each CH vector in each methylene group, no optimal value for the defocussing delay Δ can be used for every peak. We set Δ equal to $1/(4J_{CH})$, which introduces a phase difference between lines 1, 2 and 7, 8 equal to $2\pi D_{ch}\Delta$. This phase difference must be corrected for interactively

with coupling constants extraction, as described by Carlomagno et al. (1998), to avoid systematic errors.

If $J_{CH_1} + D_{CH_1} \neq J_{CH_2} + D_{CH_2}$ the transfers described in Equations 1 and 2 are still selective, as will be demonstrated in the following. In addition, $C^- H_1^\alpha H_2^\beta$ and $C^- H_1^\beta H_2^\alpha$, corresponding to the central lines (empty circles) of Figure 1A, are now excited and can be observed. These transitions are selectively transformed into the transitions $H_1^- C_\alpha H_2^\beta$, $H_1^- C_\beta H_2^\alpha$, $H_2^- C_\alpha H_1^\beta$ and $H_2^- C_\beta H_1^\alpha$ by the sequence of Figure 3A. The selective transfers for the case $J_{CH_1} + D_{CH_1} \neq J_{CH_2} + D_{CH_2}$ can be understood in the following way. The ZQ mixing Hamiltonian $\mathbf{H}_1 = \pi(J_{CH_1} + D_{CH_1})(C_x H_{1x} + C_y H_{1y}) + \pi(J_{CH_2} + D_{CH_2})(C_x H_{2x} + C_y H_{2y})$, implemented by the DIPSI sequences of Figure 3B, commutes with the two symmetry operators $\mathbf{S}_1 = C_z H_{1z} + C_z H_{2z}$ and $\mathbf{S}_2 = H_{1z} + H_{2z} + C_z$, which is the operator measuring the coherence order. The free evolution Hamiltonian before and after the mixing also commutes with $\mathbf{S}_1$ and $\mathbf{S}_2$. Therefore coherences before and after the heteronuclear TOCSY mixing, brought about by $\mathbf{H}_1$, can be classified according to both symmetry operators $\mathbf{S}_1$ and $\mathbf{S}_2$ (Levitt et al., 1985). One finds the following eigenvalues for the commutators $[S_1, \rho] = s_1\rho$ and $[S_2, \rho] = s_2\rho$:

$$
\begin{array}{lccc}
 & & & S_1 \quad S_2 \\
H_1^- C^\alpha H_2^\alpha, H_2^- C^\alpha H_1^\alpha & \longleftrightarrow & C^- H_1^\alpha H_2^\alpha : & -1 \quad -1 \\
H_1^- C^\alpha H_2^\beta, H_2^- C^\alpha H_1^\beta & \longleftrightarrow & C^- H_1^\alpha H_2^\beta : & 0 \quad -1 \\
H_1^- C^\beta H_2^\alpha, H_2^- C^\beta H_1^\alpha & \longleftrightarrow & C^- H_1^\beta H_2^\alpha : & 0 \quad -1 \\
H_1^- C^\beta H_2^\beta, H_2^- C^\beta H_1^\beta & \longleftrightarrow & C^- H_1^\beta H_2^\beta : & 1 \quad -1
\end{array}
$$

The heteronuclear TOCSY achieves transfer only between coherences which have the same eigenvalue for both the symmetry operators $\mathbf{S}_1$ and $\mathbf{S}_2$. Therefore, only the peaks shown in Figure 1B are selected by the experiment of Figure 3A. The selection rule for the experiment of Figure 4 is derived by adding a $\pi_x(^{13}C)$ pulse before and a $\pi_x(^1H)$ after the DIPSI mixing scheme, as explained above. This inverts the coherence orders before and after the mixing and in addition the spin state of the coupled proton in ω_2, yielding peaks 1 and 8 (Figure 1C). The presence of the additional peaks deriving from the $C^- H_1^\alpha H_2^\beta$ and $C^- H_1^\beta H_2^\alpha$ coherences in ω_1 increases spectral overlap but does not hinder the reliable extraction of the three $J + D$ couplings, since they appear at a different frequency in ω_1 compared to the interesting
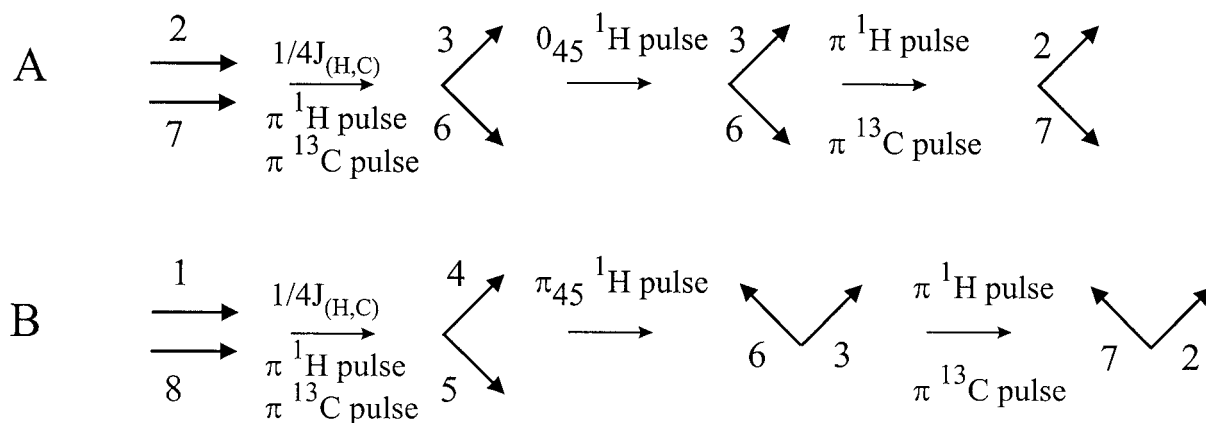
Figure 5. Pictorial explanation of the peak selection which takes place in sequences 3B and 3C after point *a*. In panel A the magnetization terms corresponding to peaks 2 and 7 are defocused with respect to the $J_{CH} + D_{CH}$ coupling for a total delay $1/(4(J_{CH} + D_{CH}))$; as a consequence they acquire a 90° phase difference in the proton dimension. In panel B inter-conversion between various lines occurs due to the presence of $\pi({}^{13}C)$ and $\pi({}^{1}H)$ pulses, as reported in the figure. The final terms are the same as those in panel A, but peak 7 has undergone a sign inversion, as desired for the S^3E selection.

traces. Moreover, in large macromolecules these peaks have a broader linewidth in ω_1 than the desired ones, due to cross-correlated relaxation Γ_{CH_1,CH_2}, and may partially cancel out depending on the relative size of the $J_{CH_1} + D_{CH_1}$ and $J_{CH_2} + D_{CH_2}$ couplings. In the oriented sample measured for the present study these peaks could not be observed, although some of the D_{CH} couplings were up to 50 Hz large.

The S^3E element does no longer work perfectly when $J_{CH} + D_{CH}$ deviates from $1/(2\Delta)$. In this case, the initial estimation of the $J_{CH} + D_{CH}$ coupling constant can be obtained from the SPITZE-HSQC spectrum. This can be used for phase correction in ω_2 for the two spectra to be added and subtracted for the S^3E selection. In this way a clean suppression of the undesired peaks is achieved.

Experimental and results

The new SPITZE-HSQC sequences have been applied to a 10 mg ${}^{13}C$, ${}^{15}N$ labeled sample of ubiquitin in a H_2O/D_2O 90/10 solution at pH 5.0 and 303 K (commercially available from VLI Research, Inc., Malvern, PA) in 5 mm NMR tubes (500 μl). All experiments were performed at 300 K on Bruker DRX 600 MHz spectrometers (Bruker AG, Rheinstetten, Germany) equipped with TXI HCN z-grad probes. Spectra were processed using FELIX 98.0 (MSI, San Diego, CA).

The spectra resulting from the pulse sequences of Figures 3 and 4 after the post-acquisition data treatment explained in the previous section are shown in

Figure 6 for the region containing the CH_2 correlations of glycines. Separation of peaks 1 and 8 has been achieved in the two spectra shown in the two upper panels, while peaks 2 and 7 are in the spectra shown in the two lower panels. The difference in the resonance frequencies of peaks 1 and 8 corresponds to $J_{CH} + D_{CH} + J_{HH} + D_{HH}$, that of peaks 2 and 7 to $J_{CH} + D_{CH} - J_{HH} - D_{HH}$ and that of peaks 1 and 2 and 7 and 8, respectively, to $J_{HH} + D_{HH}$. From the SPITZE-HSQC spectra the three coupling constants $J_{H_1 H_2} + D_{H_1 H_2}$, $J_{CH_1} + D_{CH_1}$ and $J_{CH_2} + D_{CH_2}$ can be measured for all six glycines (Table 1). The aforementioned advantages of the SPITZE-HSQC with respect to a coupled HSQC are illustrated in Figure 7. For peak 1 of the H_1 of Gly10 a gain in signal-to-noise of a factor 3 is found in the SPITZE-HSQC experiment with respect to the coupled HSQC. Moreover, in the coupled HSQC peak 8 of Gly10 overlaps with peak 1 of Gly47, hindering the extraction of the J_{CH_1}. In the novel approach peaks 1 and 8 are separated in two spectra and all J_{CH} couplings can be measured without ambiguities.

The same experiments have been repeated for 1.5 mg of ${}^{13}C$, ${}^{15}N$ labeled ubiquitin (VLI Research) dissolved in 5% CHAPSO/DLPC/CTAB (1:5:0.1) (pH 5, 10 mM phosphate buffer, 90/10 H_2O/D_2O) bicelles in Shigemi microcell tubes (250 μl) (Losonczi and Prestegard, 1998; Wang et al., 1998). Traces for residue Gly 10 are shown in Figure 8. The alignment tensor was calculated based on the X-ray and NMR structure and has been calculated with the program *Dipocoup* (Meiler et al., 2000) using ${}^{1}D_{NH}$ dipolar
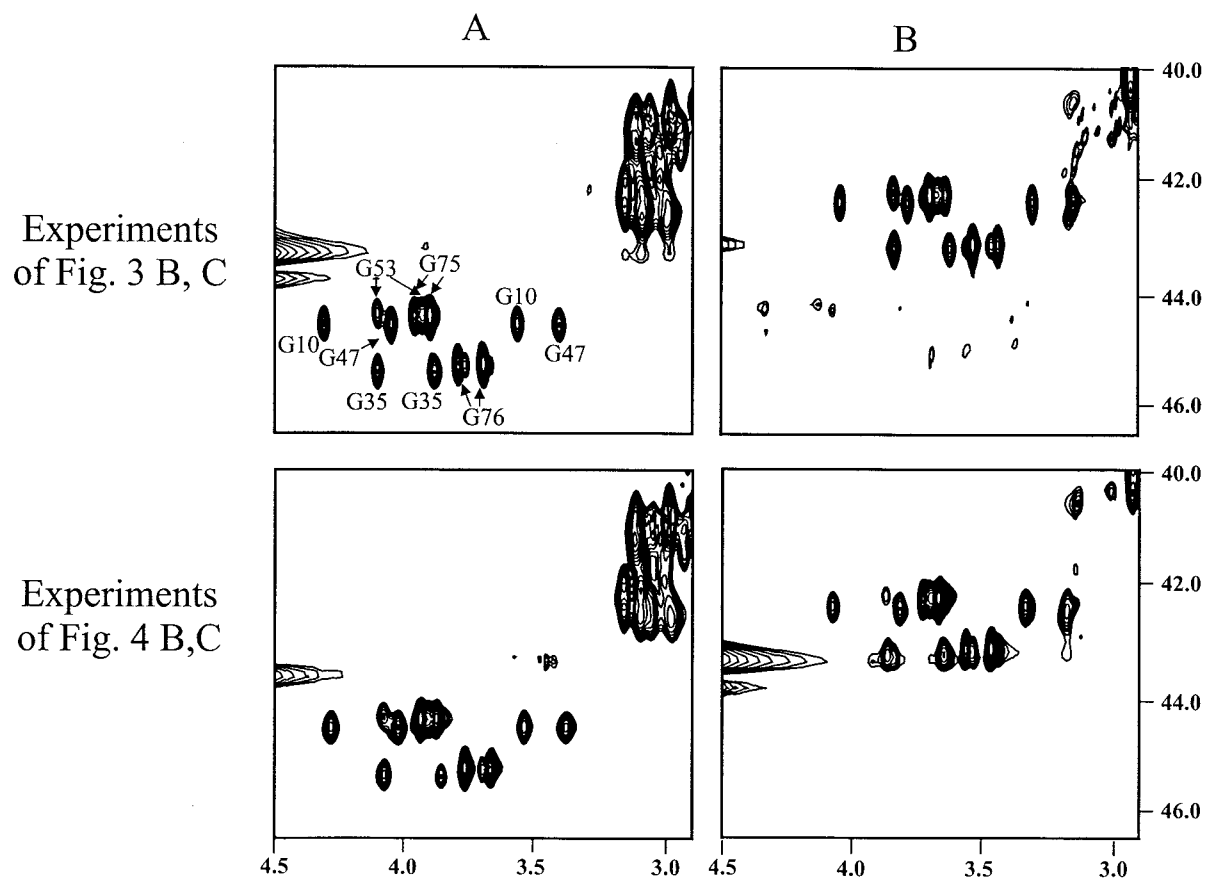
Figure 6. Spectra deriving from adding (panel A) and subtracting (panel B) the experiment of Figures 3B,C and 4B,C for a 1.5 mM sample of $^{13}C/^{15}N$ labeled ubiquitin. ^{15}N and ^{13}CO were decoupled in t_1 with 180° pulses. The region corresponding to the glycine CH_2 groups is shown. Each experiment has run for 8 h for a total of 2048×512 real points. Data were linear predicted in t_1 to 512 complex points and then zero-filled to 1024 points.
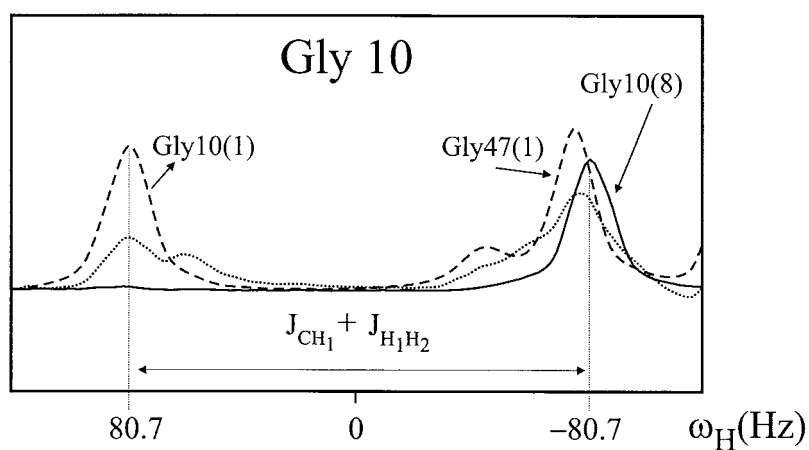

Figure 7. Traces extracted from the spectra in the upper panels of Figure 6 (dashed line: panel A; continuous line: panel B) at the C_α chemical shift of Gly10. The dotted line represents the corresponding trace in a coupled HSQC, which has run for as long as one SPITZE-HSQC sequence. The trace has been multiplied by 2 to account for the fact that the two SPITZE-HSQC experiments of Figure 4, which give rise to the corresponding dashed and continuous traces, have run together for twice as long as the HSQC experiment. In the HSQC trace peak 1 of Gly47 overlays with peak 8 of Gly10, hindering the extraction of J_{CH_1}. In the SPITZE-HSQC experiments peaks 1 and 8 are separated in two spectra and all J_{CH} couplings can be measured without ambiguities.
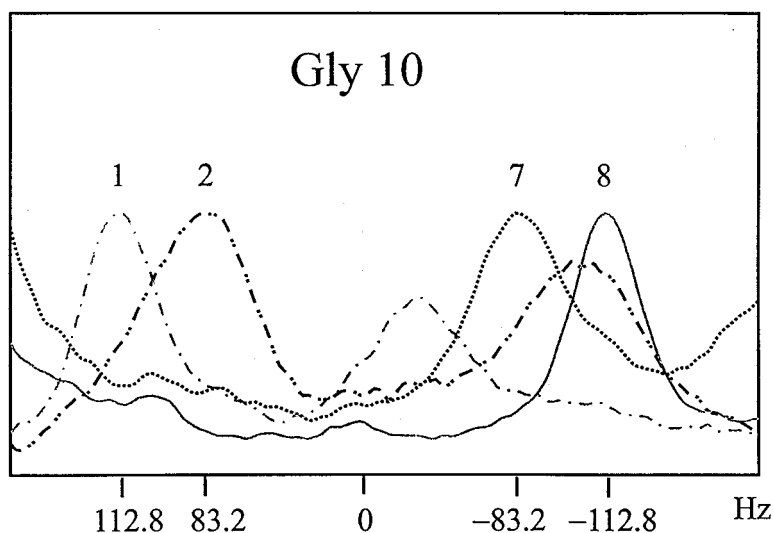
Figure 8. Traces corresponding to peaks 1 (dashed line), 2 (dashed dotted line), 7 (dotted line) and 8 (continuous line) for residue Gly 10 of ubiquitin dissolved in 5% CHAPSO/DLPC/CTAB (1:5:0.1) (pH 5 10 mM phosphate buffer, 90/10 H_2O/D_2O) bicelles at the chemical shift of proton H_1. $J_{CH} + D_{CH}$ couplings can be extracted from the chemical shift difference of lines 1 and 7 or 2 and 8, while $J_{HH} + D_{HH}$ is obtained from the chemical shift difference of lines 1 and 2 or 7 and 8.

couplings measured with the S^3E (Meissner et al., 1997) method. A total of 56 $^1D_{NH}$ dipolar couplings could be measured. The Q-factor (Cornilescu et al., 1999) of the experimental dipolar couplings compared with the one calculated from the crystal structure of ubiquitin (Vijay-Kumar et al., 1987) is 0.28, which equals a correlation coefficient of R = 0.96. The eigenvalues of the alignment tensor are defined: $D_{xx} = 11.6$ Hz, $D_{yy} = 49.3$ Hz, $D_{zz} = -60.9$ Hz ($D_{ax} = -30.5$ Hz, R = 0.41). Q is equal to 0.199 (R = 0.98) by comparison with a refined NMR structure obtained taking dipolar couplings into account (Cornilescu et al., 1999a,b) (alignment tensor: $D_{xx} = 13.8$ Hz, $D_{yy} = 47.8$ Hz, $D_{zz} = -61.6$ Hz, $D_{ax} = -30.8$ Hz, R = 0.37).

For this partially aligned sample the resonances of Gly53 are too broad to be detectable and the resonances of the two H_α protons of Gly35 are shifted under the water resonance for two of the four SPITZE-HSQC spectra. The values of the $D_{H_1H_2}$, D_{CH_1} and D_{CH_2} for the remaining four glycines are reported in Table 1, together with the theoretical values calculated from the NMR and X-ray structure. The sign of the $J_{H_1H_2} + D_{H_1H_2}$ coupling is the same as for the $J_{H_1H_2}$ coupling if the relative position of lines 1 and 2 is not inverted with respect to that of the non-oriented sample (peak 1 downfield, peak 2 upfield). All calculations of dipolar couplings have been performed with the program *DipoCoup* (Meiler et al., 2000).

The $D_{H_1H_2}$, D_{CH_1} and D_{CH_2} dipolar couplings for Gly10 and Gly47 and the $D_{H_1H_2}$ coupling for Gly35 do not agree well with the X-ray structure but better with the NMR structure. The numerical agreement is not excellent, as for other H,H dipolar coupling measurement (Cai et al., 1999; Peti and Griesinger, 2000), which reflects the presence of motion as well as deviations from the final structure. The agreement for the mentioned glycine residues can be increased assuming an order parameter of 0.85, which is in line with the order parameter measured for the NH vectors from relaxation measurements. Thus most of the deviation between measured and predicted dipolar couplings can be attributed to motion.

The measured dipolar couplings for Gly75 and Gly76 do not agree with the calculated ones due to the high degree of disorder at the C-terminal part of the molecule. The experimental value of D_{CH_1} is equal to that of D_{CH_2} for both residues, as is expected in the presence of extensive conformational averaging.

For side-chain methylene groups a lower sensitivity is expected due to the presence of $J_{CC} + D_{CC}$ couplings. While the quality of the selectivity is not affected by the presence of other carbon coupling partners, as shown in theoretical simulations and in experiments on diacetone-glucose (unpublished results), the sensitivity of the transfer will be. The mixing time $1/(\sqrt{2}J_{CH})$ is almost three times shorter than that required for a complete transfer through J_{CC} couplings.

Nevertheless, a signal-to-noise loss of up to a factor 2 can take place for non-oriented samples, and perhaps more in oriented systems, depending on the D_{CC}. In special cases selective carbon mixing sequences could be used to avoid the magnetization transfer to neighboring carbons. Moreover, resolution in the carbon dimension can be enhanced by a constant time version of the experiment or a 3D correlation.

Conclusions

We have presented a method to measure the $D_{H_1 H_2}$, D_{CH_1} and D_{CH_2} dipolar couplings in methylene moieties based on an S^3E-type correlation. The proposed experiments allow the extraction of magnitude and sign of all three dipolar couplings with minimal spectral overlap and increased signal-to-noise with respect to a coupled HSQC. The method has been demonstrated on the glycine residues of partially oriented ubiquitin. The measured dipolar couplings can be used in local structural refinements and constitute a great help in the stereospecific assignment of protons.

Acknowledgements

References

Bodenhausen, G. and Ruben, D.J. (1980) *Chem. Phys. Lett.*, **69**, 185–189.

Cai, M., Wang, H., Olejniczak, E.T., Meadows, R.P., Gunasekera, A.H., Xu, N. and Fesik, S.W. (1999) *J. Magn. Reson.*, **139**, 451–453.

Carlomagno, T., Schwalbe, H., Rexroth, A., Sørensen, O.W. and Griesinger, C. (1998) *J. Magn. Reson.*, **135**, 216–226.

Cornilescu, G., Marquardt, J.L., Ottiger, M. and Bax, A. (1999a) *PDB database*, 1D3Z.

Cornilescu, G., Marquardt, J.L., Ottiger, M. and Bax, A. (1999b) *J. Am. Chem. Soc.*, **120**, 6836–6837.

Fischer, M.W., Losonczi, J.A., Weaver, J.L. and Prestegard, J.H. (1999) *Biochemistry*, **38**, 9013–9022.

Glaser, S.J., Schulte-Herbrüggen, T., Sieveking, M., Schedletzky, O., Nielsen, N.C., Sørensen, O.W. and Griesinger, C. (1998) *Science*, **280**, 421–424.

Levitt, M.H., Radloff, C. and Ernst, R.R. (1985) *Chem. Phys. Lett.*, **114**, 435–440.

Losonczi, J.A. and Prestegard, J.H. (1998) *J. Biomol. NMR*, **12**, 447–451.

Meiler, J., Peti, W. and Griesinger, C. (2000) *J. Biomol. NMR*, in press.

Meissner, A., Duus, J.O. and Sørensen, O.W. (1997) *J. Biomol. NMR*, **10**, 89–94.

Müller, L. (1979) *J. Am. Chem. Soc.*, **101**, 4481–4484.

Ottiger, M., Delaglio, F., Marquardt, J.L., Tjandra, N. and Bax, A. (1998) *J. Magn. Reson.*, **134**, 365–369.

Peti, W. and Griesinger, C. (2000) *J. Am. Chem. Soc.*, **122**, 3975–3976.

Rucker, S.P. and Shaka, A.J. (1989) *Mol. Phys.*, **68**, 509–517.

Shaka, A.J., Lee, C.J. and Pines, A. (1988) *J. Magn. Reson.*, **77**, 274–293.

Tjandra, N. and Bax, A. (1997) *Science*, **278**, 1111–1114.

Tolman, J.R., Flanagan, J.M., Kennedy, M.A. and Prestegard, J.H. (1995) *Proc. Natl. Acad. Sci. USA*, **92**, 9279–9283.

Vijay-Kumar, S., Bugg, C.E. and Cook, W.J. (1987) *J. Mol. Biol.*, **194**, 531–544.

Wang, H., Eberstadt, M., Olejniczak, T., Meadows, R.P. and Fesik, S.W. (1998) *J. Biomol. NMR*, **12**, 443–446.